Anomalously Large Spectral Shifts near the Quantum Tunnelling Limit in Plasmonic Rulers with Subatomic Resolution

Charlie Readman,[†,‡] Bart de Nijs,[†] István Szabó,[§] Angela Demetriadou,[∥] Ryan Greenhalgh,[†,⊥] Colm Durkan,[⊥] Edina Rosta,[§] Oren A. Scherman,*[,‡] and Jeremy J. Baumberg*[,†]

[†]NanoPhotonics Centre, Cavendish Laboratory, Department of Physics, University of Cambridge, JJ Thomson Avenue, Cambridge, CB3 0HE, United Kingdom

[‡]Melville Laboratory for Polymer Synthesis, Department of Chemistry, University of Cambridge, Lensfield Road, Cambridge CB2 1EW, United Kingdom
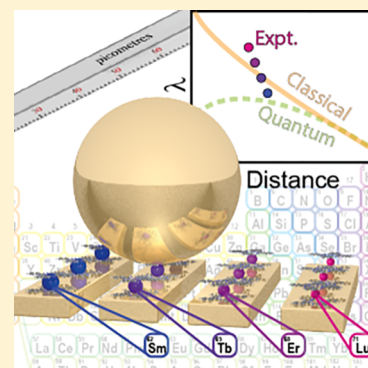
[§]Department of Chemistry, King's College London, 7 Trinity Street, London SE1 1DB, United Kingdom

[∥]School of Physics and Astronomy, University of Birmingham, Edgbaston, Birmingham, B15 2TT, United Kingdom

[⊥]The Nanoscience Centre, University of Cambridge, 11 JJ Thomson Avenue, Cambridge, CB3 0FF, United Kingdom

S *Supporting Information*

ABSTRACT: The resonance wavelength of a coupled plasmonic system is extremely sensitive to the distance between its metallic surfaces, resulting in "plasmon rulers". We explore this behavior in the subnanometer regime using self-assembled monolayers of bis-phthalocyanine molecules in a nanoparticle-on-mirror (NPoM) construct. These allow unprecedented subangstrom control over spacer thickness via choice of metal center, in a gap-size regime at the quantum-mechanical limit of plasmonic enhancement. A dramatic shift in the coupled plasmon resonance is observed as the gap size is varied from 0.39 to 0.41 nm. Existing theoretical models are unable to account for the observed spectral tuning, which requires inclusion of the quantum-classical interface, emphasizing the need for new treatments of light at the subnanoscale.

KEYWORDS: *Nanocavities, quantum plasmonics, phthalocyanines, nanoassembly, DFT, SERS*

Placing two noble metal nanostructures a short distance (<10 nm) from each other leads to electronic coupling of the collective electron oscillations (plasmons). This coupling creates a tightly confined, red-shifted and enhanced optical field within the interparticle gap, whose resonance wavelength depends strongly on the local environment.[1−3] This sensitivity has already led to applications in chemical and biological sensing,[4−6] as well as electronic devices.[7−10] One key implementation has been the plasmon ruler[11−16] in which the resonant wavelength of such a coupled system shifts predictably as the interparticle spacing (d) is varied, leading to length measurements with a much larger interaction range, longer lifetime, and greater robustness than using fluorescence resonant energy transfer (FRET).[17−19]

Plasmon rulers have been studied both experimentally[15,20,21] and theoretically[1,13,14,22] at a range of length scales. For gap sizes $d > 1$ nm, the plasmonic response can in general be modelled classically using Maxwell's equations.[1,15,23] Simplified analytical models also exist[1,24,25] as well as empirical "universal" plasmon ruler equations[11−14] that can be modified with further exponential terms to account for smaller gaps.[16] However, these models fail to describe systems with $d \lesssim 0.5$

nm at which point electron nonlocality and spillout become more dominant.[1,21,26−30]

For subnanometer gaps, this nonclassical behavior leads to a reduction or even reversal of the observed redshift with decreasing gap size.[1,21,31−33] The inherent nonlocality of electrons is accounted for with hydrodynamic terms in simplified coupling models. Electron spillout beyond the notionally sharp metal interface arises from Coulomb repulsion and electron degeneracy pressure, which can be modeled with time-dependent density functional theory (TD-DFT). Full quantum treatment, however, can only currently be implemented for small (<5 nm diameter) nanoparticles or clusters and only for simple metals like Na.[31,34−36] Additionally, for gaps within the quantum regime, $d_{QM} \approx \ln(3q\lambda\alpha/2\pi) \approx 0.4$ nm, the electron tunnelling across the gap counteracts the charge buildup on either side, diminishing the red shifts of plasmon resonant wavelength λ (here $\alpha = 1/137$ is the fine structure constant, and the semiclassical electron tunnelling wavenumber $q = \sqrt{2m\phi}/\hbar = 11$ nm^{-1} for work function of Au $\phi = 4.8$ eV).[21,27,36,37]
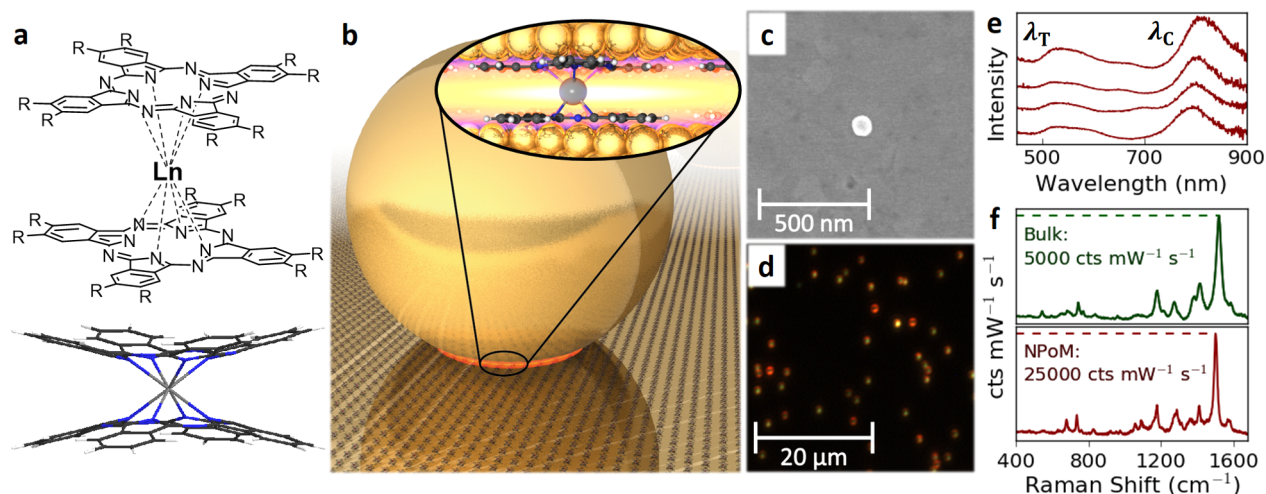
Figure 1. (a) Top: BPc* chemical structure. Ln = {Sm, Tb, Er, Lu}, R = S''C$_{12}$H$_{25}$. Bottom: geometry optimized (DFT) stick model of LuPc$_2$ with C (black), H (white), N (blue), Ln (gray), and R groups omitted for clarity. (b) Schematic of 80 nm NPoM on a full BPc* monolayer (R groups omitted). Inset shows side-view of BPc molecules in NPoM cavity. (c) SEM image of single NPoM. (d) Optical dark-field (DF) image of an ErPc*$_2$ NPoM sample. (e) Individual NPoM DF spectra (normalized, offset). (f) Top: Raman spectrum of ErPc*$_2$. Bottom: SERS spectrum of a single ErPc*$_2$ NPoM.

Despite a comprehensive focus on developing theoretical models of the quantum plasmonic regime, the number of experiments remains extremely limited. This is due to the difficulty of reliable control at such subnanometer length scales, as well as the problem of independent measurement of such gap sizes. Top-down lithographic approaches reach only down to ~5 nm before suffering from extreme irreproducibility,[12,19,38] while STM approaches are hard to combine with optics and unstable in ambient conditions.[21,39,40] Bottom-up assembly typically aims for plasmonic dimers with molecular control of the gap. A standard approach has been to use self-assembled monolayers (SAMs) of alkanethiols, the known length of which allows fine control over the spacing,[1,15,20,41] in theory creating gaps down to ~0.5 nm. However, there remains little agreement over precisely when quantum effects become important in this plasmonic gap ruler.[19,33]

To address the quantum regime more reliably, we introduce here a new class of bis-phthalocyanine (BPc) plasmonic spacers capable of fine-tuning the gap size between 0.39 and 0.41 nm around the quantum length scale d_{QM}.[42−47] These molecular spacers are sandwich complexes consisting of a central lanthanide ion and two conjugated phthalocyanine (Pc) ligands in close proximity (Figure 1a). The BPc electronic structure is dominated by the resultant π−π coupling.[42,47−53] In comparison to the previous use of graphene[2,54] as a spacer, which has a nominal 0.34 nm thickness, these BPc-based systems are stable against Au−Au van der Waals forces, physically and chemically robust, and highly suited to testing out models of conduction at optical frequencies. This also introduces a new degree of freedom into the gap, since the coupled Pc$_2$ ligand pair is easily oxidized and reduced,[47,55−59] modifying the gap electromagnetic properties. We show that the resulting plasmonic constructs are robust, scalable, and easy to fabricate via bottom-up nanoassembly. They also provide the smallest easily constructed stable nanoresonators with volumes $V_I \sim Dd^2/n_g^2 \sim 6$ nm^3.[24] We then show that existing theoretical models cannot account for the spectral tuning of the mode with such gap sizes.

This confirms the need for theories that treat coupled image dipoles and electromagnetic resonances of plasmonic metallic environments containing complex, redox-active molecules with large numbers of electrons. This also highlights the problems posed by the quantum-classical interface.

Experimental Section. While dimers are the simplest model system, they remain challenging to create in high yield (since larger-scale aggregates generally form).[5,60] As a result, we adopt a comparably simple geometry termed the nanoparticle-on-mirror (NPoM) system, in which the partner nanoparticle (NP) is replaced by a flat plasmonic surface creating analogous image charges and dipoles (Figure 1b).[2,24,61] The tightly coupled charges on either side of the gap create red-shifted coupled plasmon modes, whose spectral position is extremely sensitive to the size (d) and refractive index (n_g) of the gap.[2,24]

In the dark-field scattering spectrum of a typical NPoM construct (Figure 1e) using AuNPs of diameter D = 80 nm, two distinct plasmonic resonances are observed. First is the transverse (T) mode excited by light polarized parallel to the surface, which is located at wavelength $\lambda_T \approx 533$ nm and is barely perturbed by the properties of the spacer (because the light is concentrated outside this layer). The second, coupled (C) mode is red-shifted due to the interaction with image charges on each gap surface and is tightly confined to the nanocavity. Both the peak wavelength of the coupled resonance (λ_C) and the C/T intensity ratio (I_r) depend strongly upon the physical properties of the gap spacer, including its conductance (G); an increase in d or G causes the C mode to blue shift, while an increase in n_g leads to a red shift.[2,24,61] This sensitivity allows us to explore the optical effects of incorporating a series of BPc derivatives as NPoM molecular spacers. The BPc compounds studied here are LnPc*$_2$ (hereafter referred to as BPc*), where the lanthanide Ln = {Sm, Tb, Er, Lu} and Pc* denotes a phthalocyanine ligand octa-peripherally substituted with n-dodecylthio groups (Figure 1a) to improve solubility and encourage self-assembly on the Au surface.[45,62,63]

Results. To confirm successful assembly of these constructs (see Materials and Methods) with hotspots (Figure 1b) containing BPc* molecules, isolated NPoMs are analyzed with scanning electron microscopy (SEM), surface-enhanced
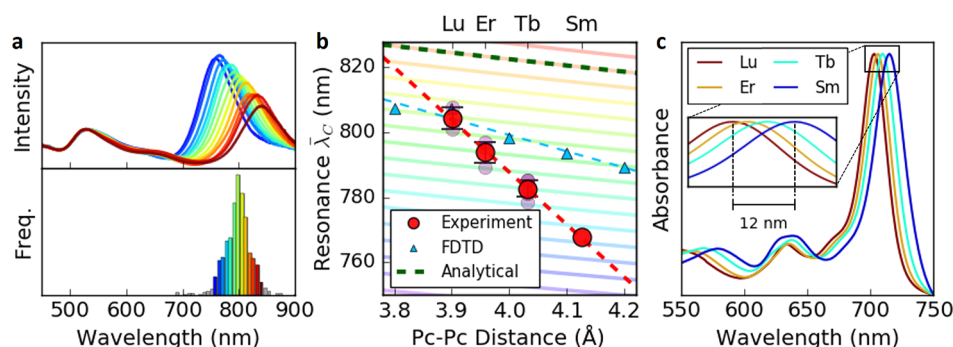
Figure 2. (a) Typical NPoM DF spectra λ_C distribution (here for ErPc*$_2$). Individual DF spectra (top) are averages of all spectra in each histogram bin of corresponding color (bottom). (b) Shift in $\overline{\lambda}_C$ with increasing size of NPoM spacer (from DFT calculations). Red circles represent average measured $\overline{\lambda}_C$ for each Ln center (individual samples are purple circles, each of 100−2000 spectra); error bars show standard deviation between samples. Solid lines show calculated shift in $\overline{\lambda}_C$ with increasing spacer thickness (using analytical model from ref 24 for $1.10 \leq n_g \leq 1.55$ ($n_g = 1.5$, green dashed line). Finite-difference time domain (FDTD) simulations are blue triangles. (c) UV−vis absorbance spectra of BPc* (10 μM in CHCl$_3$) illustrating shift in λ_α.

Raman spectroscopy (SERS) and dark-field (DF) scattering spectroscopy. SEM images (Figure 1c) reveal isolated individual NPoMs with nearest-neighbor distances larger than the optical collection spot size (∼1 μm). Significant lateral coupling between NPs is not observed at these separation distances,[13,16] so all plasmonic coupling observed is due to NP-surface interactions. Individually resolved NPoMs can be viewed under dark-field (DF) (Figure 1d) with each individual NPoM DF spectrum containing a single sharp near-infrared coupled resonance (Figure 1e). NP aggregates and NPoMs too close to be distinguished are detected and removed during postprocessing of the spectra. Comparison of NPoM SERS spectra (Figure 1f, bottom) with Raman spectra of bulk LnPc*$_2$ (Figure 1f, top) demonstrates the presence of BPc* in the optical hotspot of the nanogap. No SERS is observed when the laser is displaced off the NPoM. The combination of plasmonic field enhancement (see below) and resonant Raman effects (since BPc* has an electronic resonance around 600−700 nm[50,64]) leads to signals of ∼25 000 cts mW^{-1} s^{-1} from a single NPoM, which is large enough to enable fast dynamic SERS.

Assuming ≤100% surface coverage and a planar-lattice molecular separation of ∼3.0 nm,[62] we estimate a population of ≤95 BPc* molecules within each NPoM gap. The estimated lateral spatial intensity full-width half-maximum of the confined optical field is $\Delta x = \sqrt{Dd}/n_g$.[21] This corresponds to ∼4 nm for nanoparticle diameters $D = 80$ nm, giving an average of 10−15 BPc* molecules probed within each NPoM hotspot. This implies that SERS emission of ∼2500 cts mW^{-1} s^{-1} from each molecule is achieved in this NPoM, more than in any other system yet observed. Depending on preparation and measurement conditions, statistical variation in surface coverage will lead to significant lateral variations in the physical properties of the SAM (such as n_g) at this length scale,[40,65] with Poissonian error of ±35%. The AuNP shape/size polydispersity is also expected to cause variations in plasmonic coupling behavior across such samples.[2,61,66] This inherent variability for single nano-objects thus leads to an approximately normal distribution for λ_C.

To account for this variation, measurements of dark-field scattering spectra are collected from approximately 1000 NPoMs for each sample (Figure 2a); a vertical z-stack is performed in each case to correct for chromatic aberration.[2] Individual spectra are analyzed using a multipeak fit algorithm

and spectra containing more than one coupled plasmon resonance excluded to minimize the influence of significantly nonspherical particles.[2,54] The spectral range 450−900 nm is then divided into 80 bins (each 5.7 nm wide) and individual spectra sorted into these according to λ_C (Figure 2a, bottom). As observed previously,[2] the sharp-coupled mode resonance persists when averaging the contents of each bin (Figure 2a, top), yielding highly reproducible representative spectra with high signal-to-noise ratio. The binned frequency distribution of a sample of 1000 NPoMs typically gives a narrow Gaussian profile (Figure 2a, bottom), and the center of this gives $\overline{\lambda}_C$.

The measured $\overline{\lambda}_C$ values of 760−810 nm for samples with different Ln imply nanoparticle-surface separations of <1 nm for reasonable estimates of $n_g \approx 1.5$, based on organic monolayers.[67,68] This confirms that only a single (sub)-monolayer of BPc molecules is found in the gap, consistent with existing literature, in which STM measurements mostly reveal arrangements of BPc derivatives with Pc planes parallel to the surface and apparent height ∼0.4 nm.[45,62,63,69−71] On the basis of DFT calculations (see Supporting Information (SI) for details) and literature data,[42−44,46,47] we thus expect NP-surface separations in the range $0.3 < d < 0.5$ nm.

We first correlate these systematic spectral shifts in the dark field scattering spectra with the expected thickness of the BPc* gap as the Ln core is exchanged. DFT calculations (SI) show a slight decrease in average Pc−Pc distance (estimated as in ref 43 with increasing Ln atomic number (Z_{Ln}) for Sm → Lu. As expected, the corresponding NPoMs exhibit a redshift in $\overline{\lambda}_C$ for Sm → Lu (Figure 2b). However, both classical analytical[24] and finite-difference time domain (FDTD) calculations (Materials and Methods) suggest the slight difference in expected gap size ($\Delta d \approx 0.02$ nm) is far too small to account for the >35 nm (∼70 meV) shift in $\overline{\lambda}_C$. This robust result is the key finding here, which demands a more sophisticated understanding.

Effect of Molecular Structure. The results presented suggest deviations from classical behavior, which is indeed expected at this length scale (as discussed above). However, it is also important to consider changes in molecular properties other than height as Z_{Ln} is varied. As previously described, conductance, refractive index/polarizability, and charge transfer all influence the plasmon coupling behavior.[2,72]

BPc derivatives are strong visible light absorbers[49,73,74] and in such tightly confined plasmonic NPoM systems, strong coupling has already been observed for dyes.[72] While the UV−
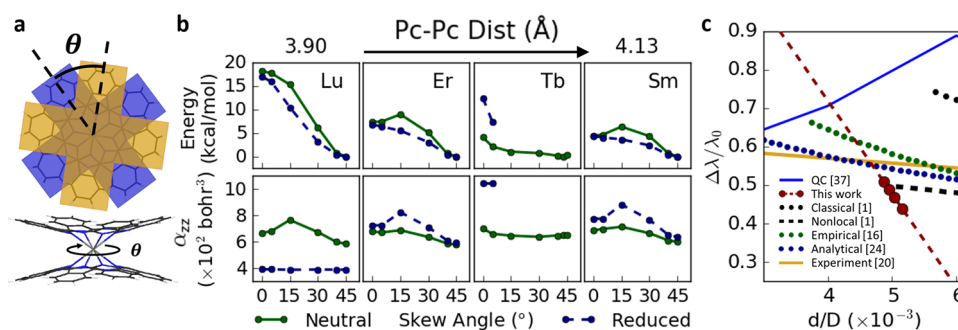
Figure 3. (a) Schematic of BPc molecule illustrating skew angle θ. (b) Variation in relative energy (top) and polarizability (bottom) with change in skew angle for $LnPc_2$ and $LnPc_2^-$ (Ln = Lu, Er, Tb, Sm). (c) Comparison of selected models from Table 1. QC = quantum corrected.

vis absorption spectra of the BPc* complexes studied here exhibit a noticeable spectral shift from Sm to Lu (Figure 2c), the range $\Delta\lambda_a \approx 12$ nm ($\Delta\nu \approx 30$ meV) is only 40% of the observed energy shift in $\overline{\lambda}_C$ and occurs in the opposite direction. The corresponding resonant refractive index is larger on the longer wavelength side of λ_a, and a quantitative model based on the measured $n_g(\lambda)$ for $TbPc_2$ thin films,[67] shifted according to λ_a(Ln), indeed confirms that this cannot account for $\Delta\lambda_C$ (Figures S2–5 and accompanying discussion). The predicted increase in n_g from Lu to Sm at the plasmon resonance decreases $\Delta\overline{\lambda}_C$ relative to our models, directly contradicted by our experimental data.

Because of the mismatch in energy and symmetry between the Ln 4f valence orbitals and those of the ligand(s) in rare earth element complexes,[42,75] Ln ions tend to behave chemically as hard ionic spheres. Because of this, the electronic structure of the BPc* complexes stems primarily from Pc−Pc orbital overlap, which is extremely sensitive to interplanar distance and skew angle θ, the relative twist between the top and bottom Pc molecules (Figure 3a).[42,47,51,76] While preliminary DFT calculations (SI) and literature data[43,47,52] suggest a staggered molecular conformation ($\theta = 45°$) in the neutral state, θ has been observed to vary with Ln size in singly reduced [BPc]$^-$ complexes.[43,67,77] Previous studies also suggest that BPc derivatives can adopt this reduced state upon contact with a metal surface.[76,78,79] Subsequent variations in θ may therefore affect the molecular polarizability and conductance.[42,51]

To investigate this hypothesis, both the energy and polarizability (z-component, parallel to the optical field in this NPoM C mode) of unsubstituted BPc molecules (Ln = Sm, Tb, Er, Lu) are calculated using DFT for a range of skew angles from 0 to 45° (Figure 3a,b; see SI for details). The overall energy barrier for rotation decreases with increasing Ln size, as expected (Figure 3b, top), due to a decrease in steric hindrance. While single-electron reduction lowers this barrier slightly, an energy minimum still exists at or near $\theta = 45°$ in all cases. The lowest activation barrier (210 meV ≈ 5 kcal/mol for $[SmPc_2]^-$) is an order of magnitude higher than the available thermal energy at room temperature (25 meV = 0.593 kcal mol^{-1} at 298 K).

While local heating in the gap might provide energy to overcome this barrier, the calculations also show a polarizability minimum at 45°, a maximum between 15° and 30°, as well as an overall increase in polarizability (and hence n_g) with increasing Ln size/interplanar distance (Figure 3b, bottom). If these differences in θ and molecular polarizability were then to significantly affect the plasmon resonance, $\Delta\overline{\lambda}_C$ would be even

smaller than that predicted by our simulations, which is the opposite of the experimental trend observed (Figure 2b).

Another consequence of the proximity of BPc is the possibility of local electron redistribution at the Au surface. Slight differences in frontier orbital energies (Figure S6) may affect the charging behavior of adsorbed BPc molecules and through electrostatic interactions, the local electron density could be affected. This would in turn affect the local plasma frequency near the gap and cause a slight shift in λ_C. A slight decrease in energy of the lowest unoccupied molecular spin orbital is observed, which is expected to have a redshifting effect from Lu to Sm (see SI for further discussion). Again, this is the opposite of the trend we observe. Interpretation of the result is further complicated by hybridization between BPc and Au electronic states,[78] which is beyond the scope here, but pertinent to effects in this subnanometer gap regime.

For variations in molecular conductance to cause the anomalous shift in $\overline{\lambda}_C$, an increase in conductance with Ln size would be required. To test this, analytical calculations were performed using the model of Benz et al.[24] with conductance allowed to vary as a polynomial function of gap size for a range of refractive index and inductance values. All scenarios require conductances on the order of 10^8–10^9 G_0. While BPc is known to exhibit (semi)conducting behavior,[55,64,69] most studies focus on dc conductance of BPc thin films or long molecular wires. This is not directly comparable to an NPoM system with a junction of single-molecule thickness, in which the relevant property is ac conductance at optical frequencies. Any conductance exhibited due to BPc semiconductivity/redox will occur at much longer time scales than optical periods of a few femtoseconds and therefore have little effect on λ_C. This is confirmed by Noda et al.[80] who observed behavior consistent with a tunneling mechanism during electrical measurements of BPc:AuNP aggregates (Ln = Tb, Lu), implying negligible conductivity ($\ll G_0$) of the molecular junctions. Conductance effects are thus not considered further as the cause of the observed λ_C tuning.

Deviation from Classical Behavior. Having eliminated molecular contributions to the $\overline{\lambda}_C$ shift, more subtle consequences of gap size variation are the most probable cause, including nonclassical effects. Models employing classical electrodynamics predict that $\overline{\lambda}_C \to \infty$ as $d \to 0$.[13,22] While this works for larger separations ($d > 2$ nm), the classical treatment fails to correctly predict coupling behaviors at smaller distances.[1] The main reasons are electron nonlocality and spillout, both of which suppress the plasmon in the gap. Solution of the quantum wave functions of electrons show that Coulomb repulsion and Fermi pressures lead to spatial

Table 1. Comparison of Relevant Literature Data Exploring the Normalised $\bar{\lambda}_C$ Tuning Rate in the Subnanometer Gap Regime[a]

method	tuning rate η (at $d/D = 0.005$)	NP size (nm)	gap size (nm)	gap n_g	reference
local[a]	−14.5	$D = 120$	$0.1 \leq d \leq 10$	1	22
local[a]	−7.1	$D = 20$	$0.1 \leq d \leq \infty$	1	82
nonlocal[a]	−3.8				
local[b]	−37.6	$D = 60$	$0.3 \leq d \leq 20$	1.8	1
nonlocal/expt[b]	−5.8				
local[a]	−17.0	$D = 50$	$0 \leq d \leq 1.5$	1	37
quantum-corrected[a]	+45.6				
expt[b]	−11.4	$D = 60$	$0.5 \leq d \leq 30$	1.8	15
expt[b]	−8.2	$D = 60$	$0.7 \leq d \leq 1.6$	1.8	20
local[b]	−6.0	$D = 60$	$0.5 \leq d \leq 1.6$	1.8	41
quantum-corrected[b]	−5.6				
expt[b]	−7.3				
local[a]	−27.7	various	various	1.33	16
expt[b]	**−121**	$D = 80$	$0.39 \leq d \leq 0.41$	1.5	this work
local[b]	−57.9				
semilocal[b]	−19.8				

[a]a = AuNP/sphere dimer; b = Au NPoM.

dispersion of electrons as gap sizes become comparable to the electron density decay length. A purely local treatment of the system is therefore no longer applicable.[1,21,31−33] Experiments performed in this regime show a broadening of the coupled plasmon resonance peak and a decrease in magnitude of $\Delta\bar{\lambda}_C$ as d decreases.[1,15,21] However, we emphasize once again that in this work the opposite is experimentally observed.

Because of the very small distance range explored here ($\Delta d \approx 0.02$ nm), electron nonlocality is unlikely to cause much variation in the spectral shift. However, quantum tunnelling becomes important for $d < 0.5$ nm.[19,21,81] As the gap sizes explored here probe the upper bounds of this tunnelling regime, electron spillout is likely to change much more dramatically with d at this length scale. Tunelling currents effectively increase the gap conductance at smaller separations, leading to a screening of the coupled plasmon mode.[24,37,61] However, as with the appearance of nonlocal effects, a decrease in the magnitude of the λ_C red shift and field enhancement is then expected, followed by a complete reversal and λ_C blue shift.[21,36,37]

A range of numerical[1,21,22,82] and analytical[1,24,35,83] models incorporating nonlocality[30,82,83] and quantum corrections for electron tunnelling[31,34−37] have already been developed. Nonlocal models often include hydrodynamic treatment of the electron gas,[1,30,81] while the quantum corrected model (QCM) accounts for electron tunnelling using TDDFT calculations.[1,34−36] When considering the latter, nanostructures of the dimensions explored in this paper ($D = 80$ nm) are still far too computationally expensive to perform a full quantum calculation. Small clusters, jellium models, and/or simpler metals like Na are therefore used.

Table 1 and Figure 3c outline theoretical and experimental data from the literature that is relevant to our system. Although the data comes from a range of different NP sizes, scaling allows suitable comparison:[13,16] using normalization of $\bar{\lambda}_C$ to λ_T and of d to D allows extraction of the tuning rate $\eta = \frac{d\lambda_r}{dx}$, where $\lambda_r \approx \bar{\lambda}_C/\lambda_T - 1$ and $x = 2d/D$.

As predicted, nonlocal and/or quantum corrections of these coupled plasmonic systems lead to smaller values of η, which is contrary to the data presented in this work. At a gap spacing of

0.4 nm ($x = 0.01$ for $D = 80$ nm) we see relative shifts in $\bar{\lambda}_C$ that are an order of magnitude larger than tuning rates predicted even by "unrealistic" classical local models.

It is worth noting that no previously published experimental realizations of these systems have more than one data point below ∼0.5 nm (if any), nor do they have such fine control over the gap thickness as the tunnelling regime is reached. Subnanometer plasmonic rulers explored thus far in the literature often rely on very few data points in the subnanometer range and extrapolate from larger distances. The highly red-shifted coupled mode we observe suggests that previous estimates of gaps for alkanethiols are incorrect, and that they change their surface configuration when exposed to the large compressive van der Waals forces inside such nanogaps. While Savage et al.[21] explore this regime with a Au AFM tip dimer, the AuNP sizes involved ($D \approx 300$ nm) are significantly larger than those explored here and the tunnelling regime is approached differently, requiring applied force to displace trapped water molecules and achieve full metallic contact. So far, anomalous spectral shifts of this magnitude have not been observed. In a simple model of tunnelling through a vacuum gap, the conductivity is given by $\sigma \propto \exp\{-2qd\} = \exp\{-d/0.045 \text{ nm}\}$;[21] the corresponding fractional change in tunnelling conductivity for $\Delta d \approx 0.02$ nm is $\Delta\sigma/\sigma \sim \exp\{-0.02/0.045\} = 0.64$. A simple estimate of how this would affect the plasmon coupled mode around the critical conductance from ref 61 is given by $\frac{\partial\lambda_C}{\partial(\sigma/G_0)} = 40$ nm, suggesting shifts of $\Delta\lambda_C = 26$ nm. Although this is comparable to the shift observed in our experiments, we again note that the sign of the effect is reversed; quantum tunnelling would be expected to reduce, rather than increase, the tuning rate within this regime. We are thus forced to conclude that in such planar conducting molecular systems in plasmonic gaps in the quantum regime, there are new effects not yet predicted by any theoretical model.

The implication of our work suggests caution is needed when exploring the applicability of nm-scale plasmon rulers. When investigating the response of coupled plasmonic systems to geometrical changes, the influence of subtle chemical changes cannot be neglected. The data presented here

demonstrates that chemical composition has a more pronounced effect than previously thought. This may occur via properties beyond refractive index and conductance, where such properties are relevant at this few-molecule subnanometer scale. The combination of molecular spacers, the tuning of their electronic states, and well-defined metallic architectures points to the clear need for improved theory combining molecules and plasmonics.

In conclusion, a subnanometer plasmon ruler with unprecedented sub-Å fine-control of gap size is assembled experimentally using rare-earth bis-phthalocyanine derivatives with different metal centers in a nanoparticle-on-mirror system. The small gap size produces highly red-shifted coupled modes with large field enhancements that result in very large SERS enhancements. An anomalously large spectral shift is observed as the size of the central Ln ion is varied, with a magnitude unable to be predicted by local numerical or analytical models. Effects of variation in molecular properties and structure are found unable to explain the data, instead leading to reduction of predicted tuning rates. These gap spacings are well within the nonlocal regime and small enough that quantum tunnelling effects are expected to be non-negligible. However, current understandings of quantum corrections to these plasmonic systems also give a reduction rather than an enhancement in the tuning rate with decreasing gap size, against what is observed. We emphasize that the data presented here is reproducible across thousands of individual NPoMs and multiple sample preparations. We speculate that coupling of conjugated organic π-systems with electrons in the nearby Au across a wide range of wavevectors leads to subtle changes in the quantum tunnelling dependence and the plasmonic tuning. It is also likely that that the understanding of refractive index as a continuum complex variable is no longer possible at this atomic scale. New treatments of light at the subnanometre scale are thus demanded.

Materials and Methods. *BPc* Synthesis.* BPc* compounds were synthesized according to a two-step procedure adapted from that of Ban et al.[64]

4,5-Bis(dodecylthio)phthalonitrile. 4,5-dichlorophthalonitrile (5.295 g, 26.88 mmol) and 1-dodecanethiol (15.5 mL, 64.7 mmol) were added to anhydrous DMSO (125 mL) and purged with N_2 at 100 °C with stirring for 15 min. Finely powdered anhydrous K_2CO_3 (35 g, 250 mmol) was added to the stirred reaction mixture in 7 g portions every 5 min. The mixture was then stirred at 100 °C for a further 30 min. The red/brown mixture was cooled to room temperature, diluted with deionized water (300 mL) and extracted with $CHCl_3$ (5 × 100 mL). The combined organic extract was washed with deionized water (3 × 170 mL) and dried over $MgSO_4$. After removal of the solvent, the crude product was purified by column chromatography [silica gel; DCM/petroleum ether (bpt 40−60 °C), 60:40 v/v] and recrystallized twice from *n*-hexane to yield 4,5-bis(dodecylthio)phthalonitrile (11.62 g, 81.75%) as fluffy, off-white, plate-like crystals.

LuPc*₂. A stirred mixture of 4,5-bis(dodecylthio)-phthalonitrile (1.38 g, 2.61 mmol), lutetium acetate hydrate (0.137 g, 0.389 mmol) and 1,8-diazabicyclo[5.4.0]undec-7-ene (DBU) (0.143 mL, 0.956 mmol) in 1-hexanol (30 mL) was refluxed for 20 h under N_2 with molecular sieves. The dark green/black solution was cooled to room temperature and precipitated with MeOH. The waxy crude product was collected by vacuum filtration, washed with cold MeOH, purified three times by column chromatography [silica gel;

DCM/petroleum ether (bpt 40−60 °C), 30:70 v/v] and recrystallized four times from ethyl acetate. The product was dried under high vacuum with heating to yield LuPc*₂ (251 mg, 17.5%) as a waxy green/black solid. ErPc*₂, TbPc*₂, and SmPc*₂ were prepared from the respective $Ln(OAc)_3$ precursors using the same method. See SI for full details and characterization.

Sample Preparation. Template-stripped gold (TSG) substrates were prepared as follows: a Si wafer was cleaned with a Decon 90 solution and rinsed with isopropanol, ethanol, and deionized water. Au was then evaporated at a rate of 1 Å s^{-1}, to a thickness of 200 nm. Small Si pieces (∼1 cm^2) were attached to the exposed Au with Epo-Tek 377 epoxy resin, cured at 150 °C and cooled to room temperature gradually (0.5 °C/min) to minimize strain in the Au layer. Each substrate was lifted off immediately prior to each use to expose a clean Au surface. Fresh TSG samples were immersed in a 1 mM solution of BPc* in *n*-hexane. After 10−90 min, the TSG was removed, rinsed with *n*-hexane and dried with compressed N_2. Samples were exposed to AuNP solution (80 nm, citrate-capped) for 30 s, rinsed with distilled water and dried again with compressed N_2.

Dark-field Analysis. Individual NPoMs were illuminated with incoherent white light at an annular illumination angle (α) of 63−75°; scattered light was collected with an angle (β) of <63°. A white scattering substrate was used as a reference. Automated data collection was performed using particle tracking code written in Python.[2] The program first identifies NPoMs within a given sample area for detailed optical analysis. To correct for chromatic aberration and different NPoM focal heights (z), multiple spectra are collected over a $\Delta z \approx 5\ \mu m$ range for each NPoM and appropriately combined. The optimum focal position for each wavelength is obtained by fitting a Gaussian function to the depth-dependent scattering intensity.

Computational Details. For full computational details, see SI. Geometry optimizations and polarizability calculations were performed for gas-phase $LnPc_2$ and $[LnPc_2]^-$. The effect of skew angle on polarizability and overall energy was explored. Finite-difference time-domain simulations were also used to calculate the expected far-field scattering mode spectra. The gap height was meshed with 24 cells to ensure that the plasmon was well resolved in the gap, while the meshing for the NP was 1 nm. The spacer was modeled with refractive index n = 1.5. Semilocal analytical calculations were performed using the model formulated by Benz et al.[24]

◼ ASSOCIATED CONTENT

ⓢ Supporting Information

The Supporting Information is available free of charge on the ACS Publications website at DOI: 10.1021/acs.nano-lett.9b00199.

> Additional computational details. Full synthesis/characterization details. BPc* UV−vis absorption spectra. Example STM image of TbPc*₂ on Au. (PDF)

◼ AUTHOR INFORMATION

Corresponding Authors

*E-mail: (J.J.B.) jjb12@cam.ac.uk..
*E-mail: (O.A.S.) oas23@cam.ac.uk

ORCID 🔬

István Szabó: 0000-0002-3700-3614

Angela Demetriadou: 0000-0001-7240-597X
Edina Rosta: 0000-0002-9823-4766
Oren A. Scherman: 0000-0001-8032-7166
Jeremy J. Baumberg: 0000-0002-9606-9488

Notes

◼ ACKNOWLEDGMENTS

◼ REFERENCES

(1) Ciracì, C.; Hill, R. T.; Mock, J. J.; Urzhumov, Y.; Fernández-Domínguez, A. I.; Maier, S. A.; Pendry, J. B.; Chilkoti, A.; Smith, D. R. *Science* **2012**, *337*, 1072−1074.

(2) de Nijs, B.; Bowman, R. W.; Herrmann, L. O.; Benz, F.; Barrow, S. J.; Mertens, J.; Sigle, D. O.; Chikkaraddy, R.; Eiden, A.; Ferrari, A.; et al. *Faraday Discuss.* **2015**, *178*, 185−193.

(3) Wang, H. *Sci. Rep.* **2018**, *8*, 9589.

(4) Kasera, S.; Biedermann, F.; Baumberg, J. J.; Scherman, O. A.; Mahajan, S. *Nano Lett.* **2012**, *12*, 5924−5928.

(5) Kasera, S.; Herrmann, L. O.; del Barrio, J.; Baumberg, J. J.; Scherman, O. A. *Sci. Rep.* **2015**, *4*, 6785.

(6) Sigle, D. O.; Kasera, S.; Herrmann, L. O.; Palma, A.; de Nijs, B.; Benz, F.; Mahajan, S.; Baumberg, J. J.; Scherman, O. A. *J. Phys. Chem. Lett.* **2016**, *7*, 704.

(7) Di Martino, G.; Sonnefraud, Y.; Kéna-Cohen, S.; Tame, M.; Ozdemir, S. K.; Kim, M. S.; Maier, S. A. *Nano Lett.* **2012**, *12*, 2504−2508.

(8) Bozhevolnyi, S. I.; Volkov, V. S.; Devaux, E.; Laluet, J.-Y.; Ebbesen, T. W. *Nature* **2006**, *440*, 508.

(9) Ozbay, E. *Science* **2006**, *311*, 189−193.

(10) Zia, R.; Schuller, J. A.; Chandran, A.; Brongersma, M. L. *Mater. Today* **2006**, *9*, 20−27.

(11) Reinhard, B. M.; Siu, M.; Agarwal, H.; Alivisatos, A. P.; Liphardt, J. *Nano Lett.* **2005**, *5*, 2246−2252.

(12) Jain, P. K.; Huang, W.; El-Sayed, M. A. *Nano Lett.* **2007**, *7*, 2080−2088.

(13) Ben, X.; Park, H. S. *J. Phys. Chem. C* **2011**, *115*, 15915−15926.

(14) Ben, X.; Park, H. S. *J. Phys. Chem. C* **2012**, *116*, 18944−18951.

(15) Hill, R. T.; Mock, J. J.; Hucknall, A.; Wolter, S. D.; Jokerst, N. M.; Smith, D. R.; Chilkoti, A. *ACS Nano* **2012**, *6*, 9237−9246.

(16) Dolinnyi, A. I. *J. Phys. Chem. C* **2015**, *119*, 4990−5001.

(17) Sönnichsen, C.; Reinhard, B. M.; Liphardt, J.; Alivisatos, A. P. *Nat. Biotechnol.* **2005**, *23*, 741.

(18) Lerch, S.; Reinhard, B. M. *Adv. Mater.* **2016**, *28*, 2030−2036.

(19) Lerch, S.; Reinhard, B. M. *Int. J. Mod. Phys. B* **2017**, *31*, 1740002.

(20) Hajisalem, G.; Min, Q.; Gelfand, R.; Gordon, R. *Opt. Express* **2014**, *22*, 9604−9610.

(21) Savage, K. J.; Hawkeye, M. M.; Esteban, R.; Borisov, A. G.; Aizpurua, J.; Baumberg, J. J. *Nature* **2012**, *491*, 574−577.

(22) Romero, I.; Aizpurua, J.; Bryant, G. W.; De Abajo, F. J. G. *Opt. Express* **2006**, *14*, 9988−9999.

(23) Myroshnychenko, V.; Rodríguez-Fernández, J.; Pastoriza-Santos, I.; Funston, A. M.; Novo, C.; Mulvaney, P.; Liz-Marzan, L. M.; de Abajo, F. J. G. *Chem. Soc. Rev.* **2008**, *37*, 1792−1805.

(24) Benz, F.; de Nijs, B.; Tserkezis, C.; Chikkaraddy, R.; Sigle, D. O.; Pukenas, L.; Evans, S. D.; Aizpurua, J.; Baumberg, J. J. *Opt. Express* **2015**, *23*, 33255−33269.

(25) Aubry, A.; Lei, D. Y.; Maier, S. A.; Pendry, J. B. *ACS Nano* **2011**, *5*, 3293−3308.

(26) David, C.; García de Abajo, F. J. *J. Phys. Chem. C* **2011**, *115*, 19470−19475.

(27) Dong, T.; Ma, X.; Mittra, R. *Appl. Phys. Lett.* **2012**, *101*, 233111.

(28) Teperik, T. V.; Nordlander, P.; Aizpurua, J.; Borisov, A. G. *Opt. Express* **2013**, *21*, 27306−27325.

(29) Teperik, T. V.; Nordlander, P.; Aizpurua, J.; Borisov, A. G. *Phys. Rev. Lett.* **2013**, *110*, 263901.

(30) Ciracì, C.; Urzhumov, Y.; Smith, D. R. *J. Opt. Soc. Am. B* **2013**, *30*, 2731−2736.

(31) Zuloaga, J.; Prodan, E.; Nordlander, P. *Nano Lett.* **2009**, *9*, 887−891.

(32) Zhu, W.; Crozier, K. B. *Nat. Commun.* **2014**, *5*, 5228.

(33) Zhu, W.; Esteban, R.; Borisov, A. G.; Baumberg, J. J.; Nordlander, P.; Lezec, H. J.; Aizpurua, J.; Crozier, K. B. *Nat. Commun.* **2016**, *7*, 11495.

(34) Scholl, J. A.; García-Etxarri, A.; Koh, A. L.; Dionne, J. A. *Nano Lett.* **2013**, *13*, 564−569.

(35) David, C.; García de Abajo, F. J. *ACS Nano* **2014**, *8*, 9558−9566.

(36) Esteban, R.; Zugarramurdi, A.; Zhang, P.; Nordlander, P.; García-Vidal, F. J.; Borisov, A. G.; Aizpurua, J. *Faraday Discuss.* **2015**, *178*, 151−183.

(37) Esteban, R.; Borisov, A. G.; Nordlander, P.; Aizpurua, J. *Nat. Commun.* **2012**, *3*, 825.

(38) Halas, N. J.; Lal, S.; Chang, W.-S.; Link, S.; Nordlander, P. *Chem. Rev.* **2011**, *111*, 3913−3961.

(39) Berndt, R.; Gimzewski, J. K.; Schlittler, R. R. *Ultramicroscopy* **1992**, *42*, 355−359.

(40) Vilan, A.; Aswal, D.; Cahen, D. *Chem. Rev.* **2017**, *117*, 4248−4286.

(41) Hajisalem, G.; Nezami, M. S.; Gordon, R. *Nano Lett.* **2014**, *14*, 6651−6654.

(42) Rousseau, R.; Aroca, R.; Rodriguez-Mendez, M. L. *J. Mol. Struct.* **1995**, *356*, 49−62.

(43) Koike, N.; Uekusa, H.; Ohashi, Y.; Harnoode, C.; Kitamura, F.; Ohsaka, T.; Tokuda, K. *Inorg. Chem.* **1996**, *35*, 5798−5804.

(44) Deng, Z.; Rauschenbach, S.; Stepanow, S.; Klyatskaya, S.; Ruben, M.; Kern, K. *Phys. Scr.* **2015**, *90*, 098003.

(45) Otsuki, J. *Supramol. Chem.* **2011**, *23*, 169−182.

(46) Miyake, K.; Fukuta, M.; Asakawa, M.; Hori, Y.; Ikeda, T.; Shimizu, T. *J. Am. Chem. Soc.* **2009**, *131*, 17808−17813.

(47) Qi, D.; Zhang, L.; Wan, L.; Zhang, Y.; Bian, Y.; Jiang, J. *Phys. Chem. Chem. Phys.* **2011**, *13*, 13277−13286.

(48) Bixner, O.; Lukeš, V.; Mančal, T.; Hauer, J.; Milota, F.; Fischer, M.; Pugliesi, I.; Bradler, M.; Schmid, W.; Riedle, E.; et al. *J. Chem. Phys.* **2012**, *136*, 204503.

(49) Prall, B. S.; Parkinson, D. Y.; Fleming, G. R.; Yang, M.; Ishikawa, N. *J. Chem. Phys.* **2004**, *120*, 2537−2540.

(50) Prall, B. S.; Parkinson, D. Y.; Ishikawa, N.; Fleming, G. R. *J. Phys. Chem. A* **2005**, *109*, 10870−10879.

(51) Komeda, T.; Isshiki, H.; Liu, J.; Zhang, Y.-F.; Lorente, N.; Katoh, K.; Breedlove, B. K.; Yamashita, M. *Nat. Commun.* **2011**, *2*, 217.

(52) Kahlal, S.; Mentec, A.; Pondaven, A.; L'Her, M.; Saillard, J.-Y. *New J. Chem.* **2009**, *33*, 574−582.

(53) Ishikawa, N.; Ohno, O.; Kaizu, Y.; Kobayashi, H. *J. Phys. Chem.* **1992**, *96*, 8832−8839.

(54) Mertens, J.; Eiden, A. L.; Sigle, D. O.; Huang, F.; Lombardo, A.; Sun, Z.; Sundaram, R. S.; Colli, A.; Tserkezis, C.; Aizpurua, J.; et al. *Nano Lett.* **2013**, *13*, 5033−5038.

(55) Maitrot, M.; Guillaud, G.; Boudjema, B.; André, J.-J.; Strzelecka, H.; Simon, J.; Even, R. *Chem. Phys. Lett.* **1987**, *133*, 59−62.

(56) Liu, Y.; Shigehara, K.; Hara, M.; Yamada, A. *J. Am. Chem. Soc.* **1991**, *113*, 440−443.

(57) Rodriguez-Mendez, M. L.; Aroca, R.; DeSaja, J. A. *Chem. Mater.* **1993**, *5*, 933−937.

(58) de Saja, J. A.; Rodríguez-Méndez, M. L. *Adv. Colloid Interface Sci.* **2005**, *116*, 1−11.

(59) Wulan, Q.; Kitamura, F. *Bull. Chem. Soc. Jpn.* **2007**, *80*, 1740−1745.

(60) Taylor, R. W.; Lee, T.-C.; Scherman, O. A.; Esteban, R.; Aizpurua, J.; Huang, F. M.; Baumberg, J. J.; Mahajan, S. *ACS Nano* **2011**, *5*, 3878−3887.

(61) Benz, F.; Tserkezis, C.; Herrmann, L. O.; de Nijs, B.; Sanders, A.; Sigle, D. O.; Pukenas, L.; Evans, S. D.; Aizpurua, J.; Baumberg, J. J. *Nano Lett.* **2015**, *15*, 669−674.

(62) Klymchenko, A. S.; Sleven, J.; Binnemans, K.; De Feyter, S. *Langmuir* **2006**, *22*, 723−728.

(63) Yang, Z.-Y.; Gan, L.-H.; Lei, S.-B.; Wan, L.-J.; Wang, C.; Jiang, J.-Z. *J. Phys. Chem. B* **2005**, *109*, 19859−19865.

(64) Ban, K.; Nishizawa, K.; Ohta, K.; van de Craats, A. M.; Warman, J. M.; Yamamoto, I.; Shirai, H. *J. Mater. Chem.* **2001**, *11*, 321−331.

(65) Akkerman, H. B.; Blom, P. W. M.; De Leeuw, D. M.; De Boer, B. *Nature* **2006**, *441*, 69.

(66) Byers, C. P.; Hoener, B. S.; Chang, W.-S.; Yorulmaz, M.; Link, S.; Landes, C. F. *J. Phys. Chem. B* **2014**, *118*, 14047−14055.

(67) Robaschik, P.; Fronk, M.; Toader, M.; Klyatskaya, S.; Ganss, F.; Siles, P. F.; Schmidt, O. G.; Albrecht, M.; Hietschold, M.; Ruben, M.; et al. *J. Mater. Chem. C* **2015**, *3*, 8039−8049.

(68) Seidel, F.; Fronk, M.; Himcinschi, C.; Chis, V.; Zahn, D. R. T. *Phys. Status Solidi C* **2010**, *7*, 222−226.

(69) Katoh, K.; Yoshida, Y.; Yamashita, M.; Miyasaka, H.; Breedlove, B. K.; Kajiwara, T.; Takaishi, S.; Ishikawa, N.; Isshiki, H.; Zhang, Y. F.; et al. *J. Am. Chem. Soc.* **2009**, *131*, 9967−9976.

(70) Glebe, U.; Weidner, T.; Baio, J. E.; Schach, D.; Bruhn, C.; Buchholz, A.; Plass, W.; Walleck, S.; Glaser, T.; Siemeling, U. *ChemPlusChem* **2012**, *77*, 889−897.

(71) Siemeling, U.; Schirrmacher, C.; Glebe, U.; Bruhn, C.; Baio, J. E.; Árnadóttir, L.; Castner, D. G.; Weidner, T. *Inorg. Chim. Acta* **2011**, *374*, 302−312.

(72) Chikkaraddy, R.; de Nijs, B.; Benz, F.; Barrow, S. J.; Scherman, O. A.; Rosta, E.; Demetriadou, A.; Fox, P.; Hess, O.; Baumberg, J. J. *Nature* **2016**, *535*, 127.

(73) de la Torre, G.; Claessens, C. G.; Torres, T. *Chem. Commun.* **2007**, *20*, 2000−2015.

(74) Yoshino, K.; Lee, S. B.; Sonoda, T.; Kawagishi, H.; Hidayat, R.; Nakayama, K.; Ozaki, M.; Ban, K.; Nishizawa, K.; Ohta, K.; et al. *J. Appl. Phys.* **2000**, *88*, 7137−7143.

(75) Ishikawa, N.; Sugita, M.; Okubo, T.; Tanaka, N.; Iino, T.; Kaizu, Y. *Inorg. Chem.* **2003**, *42*, 2440−2446.

(76) Fu, Y.-S.; Schwöbel, J.; Hla, S.-W.; Dilullo, A.; Hoffmann, G.; Klyatskaya, S.; Ruben, M.; Wiesendanger, R. *Nano Lett.* **2012**, *12*, 3931−3935.

(77) Hückstädt, H.; Tutaß, A.; Göldner, M.; Cornelissen, U.; Homborg, H. *Z. Anorg. Allg. Chem.* **2001**, *627*, 485−497.

(78) Vitali, L.; Fabris, S.; Conte, A. M.; Brink, S.; Ruben, M.; Baroni, S.; Kern, K. *Nano Lett.* **2008**, *8*, 3364−3368.

(79) Pan, Y.; Kanisawa, K.; Ishikawa, N.; Fölsch, S. *J. Phys.: Condens. Matter* **2017**, *29*, 364001.

(80) Noda, Y.; Noro, S.; Akutagawa, T.; Nakamura, T. *Sci. Rep.* **2015**, *4*, 3758.

(81) Toscano, G.; Straubel, J.; Kwiatkowski, A.; Rockstuhl, C.; Evers, F.; Xu, H.; Mortensen, N. A.; Wubs, M. *Nat. Commun.* **2015**, *6*, 7132.

(82) Garcia de Abajo, F. J. *J. Phys. Chem. C* **2008**, *112*, 17983−17987.

(83) Luo, Y.; Fernandez-Dominguez, A. I.; Wiener, A.; Maier, S. A.; Pendry, J. B. *Phys. Rev. Lett.* **2013**, *111*, 93901.